Indian Journal of Pure & Applied Physics
Vol. 58, April 2020, pp. 282-293

Monitoring mixed neutron-proton field near the primary proton and deuteron beams in spallation targets

P Tichý [a,b,c*], J Adam[a,d], A A Baldin[a,e], P Chudoba[b], W I Furman[a], S A Gustov[a], J H Khushvaktov[a,f], A Krása[g], M Majerle[b], I I Mar'in[a], A A Solnyshkin[a], M Suchopár[h], J Svoboda[a,d], O Svoboda[b] , S I Tyutyunnikov[a], J Vrzalová[a,b], V Wagner[b,c], L Závorka[i] & M Zeman[a,d]

[a]Joint Institute for Nuclear Research, Joliot-Curie 6, Dubna 141980, Russia

[b]Nuclear Physics Institute of the CAS, Hlavní 130, Řež near Prague 25068, Czech Republic

[c]Faculty of Nuclear Sciences and Physical Engineering, Czech Technical University in Prague, Břehová 7, Prague 11519, Czech Republic

[d]Faculty of Electrical Engineering and Communication, Brno University of Technology, Technická 3058/10, Brno 61600, Czech Republic

[e]Institute for Advanced Studies "OMEGA", Universitetskaya 19, Dubna 141980, Russia

[f]Institute of Nuclear Physics ASRU, Tashkent 100214, Uzbekistan

[g]Belgian Nuclear Research Centre SCK-CEN, Boeretang 200, Mol 2400, Belgium

[h]ÚJV Řež, Hlavní 130, Řež near Prague 25068, Czech Republic

[i]Los Alamos National Laboratory, P.O. Box 1663, Los Alamos NM 87545, United States

Received 17 February 2020

At the Joint Institute for Nuclear Research (JINR) we are involved in the Accelerator-Driven-System (ADS) research. We perform experiments with assemblies composed of a spallation target and a subcritical blanket irradiated with high-energy proton or deuteron beams that generate high-energy neutron fields by spallation and fission reactions. In this paper, three uranium assemblies are presented: Energy plus Transmutation (E+T), QUINTA and BURAN. We discuss the results of the E+T and QUINTA irradiations by 1.6 GeV deuterons and 660 MeV protons, respectively. We have focused on the regions close to the primary beam passage through the targets. The field has been measured using activation detectors of ^{209}Bi, ^{59}Co, and ^{nat}Pb. Monte Carlo simulations using MCNPX 2.7.0 have been performed and compared to the experimental results. We discovered that the field intensity near the primary beam is very dependent on the precision of the accelerator beam settings. Therefore, a Monte Carlo-based study of the influence of the uncertainty of primary proton beam parameters on experimental result accuracy of the QUINTA assembly has been carried out. The usage of MCNPX 2.7.0 in the future BURAN irradiations has been assessed.

Keywords: Accelerator-driven systems (ADS), Subcritical assembly, Neutron flux, Monte Carlo, Activation technique, High-energy beam, Phasotron, Nuclotron

1 Introduction

The ADS research at JINR goes back far in history. Already in the 1960s, R. G. Vasilkov studied neutron production in shattering reactions in very large lead targets irradiated with relativistic protons[1]. Its new stage started in the 1990s and continues up to now. At JINR we concentrate on irradiation of assemblies, composed of a spallation target and a subcritical blanket, with high-energy proton or deuteron beams produced by the JINR Nuclotron[2] or Phasotron[3] accelerators. The aim of the experiments is the study of neutron spatial and energetic distributions inside the assemblies, production and transport of other secondary particles, transmutation of long-lived actinides, and verification of Monte Carlo simulation codes.

One of the first ADS research assemblies of the above mentioned new stage was called GAMMA-2[4]. The assembly was composed of a lead target with a diameter of 8 cm and length of 20 cm (prolonged to 50 cm later) and a paraffin blanket of 6 cm thickness that served as a neutron moderator. The GAMMA-2 successor was the GAMMA-3 assembly[5] composed of a 60 cm long lead target with a diameter of 8 cm. The target was surrounded by a massive graphite square moderator of dimensions 60×110×110 cm. The following assemblies were E+T[6], composed of a lead target and a natural uranium blanket, and a

*Corresponding author (E-mail: tichy@jinr.ru)

similar assembly QUINTA[7], which differs from E+T mainly by using the natural uranium as a spallation target instead of lead. The most recent assembly is called BURAN[7], which is composed of 20 tons of depleted uranium.

Due to spallation and fission reactions, a high-intensity neutron field is generated inside the assemblies. The neutron (but also proton and deuteron) distribution can be effectively measured by activation detectors. An advantage of activation detectors is their small dimensions so that they can be easily inserted into the assemblies in various positions. When a neutron, proton, or deuteron impinges on an activation detector, it can induce a nuclear reaction. Radionuclides formed are not stable, and they tend to decay by β radiation (products of some activation detectors like ^{nat}U or ^{232}Th also decay by α radiation). The process is accompanied by γ radiation, which is consequently measured by high-purity germanium (HPGe) detectors. By analysis of measured spectra and gamma-spectrometry methods, it is possible to gain a number of radionuclides created.

We present selected results of Bi isotopes' production in ^{209}Bi activation samples from the E+T irradiation by the 1.6 GeV deuteron beam of the Nuclotron. The influence of the precision of accelerator beam settings on the results was discovered, and therefore, an investigation of the region near the primary beam passage in the QUINTA irradiation by the 660 MeV protons of the Phasotron (using ^{59}Co and ^{nat}Pb activation samples) was performed. Eventually, we demonstrated the usage of the Monte Carlo code MCNPX 2.7.0 for the future BURAN assembly experiments.

2 Materials and Methods

2.1 Energy plus transmutation assembly (E+T)

It is composed of a lead target 480 mm long and 84 mm in diameter with a mass of 28.66 kg and a hexagonal blanket with a mass of natural uranium of 206.4 kg. E+T is divided into four sections, which are composed of 30 uranium rods. Each rod is 104 mm long, 36 mm in diameter and 1.72 kg in weight, and is encapsulated in an aluminum casing. Between every two sections, there is an 8 mm gap for detectors' placement. The E+T assembly is shown in Figs 1 and 2. The target is surrounded by a wooden shielding with dimensions 1000×1060×1100 mm^3. Inside the wooden box walls, there is a granulated polyethylene with boron carbide, and on the inner walls, there is a cadmium layer of 1 mm thickness. The box floor is covered by a 30 mm-thick textolite layer. The polyethylene moderates fast neutrons escaping the target. After the moderation, the neutrons can be absorbed in boron or the cadmium layer. A more detailed description of the E+T assembly is given, e.g. in[6].

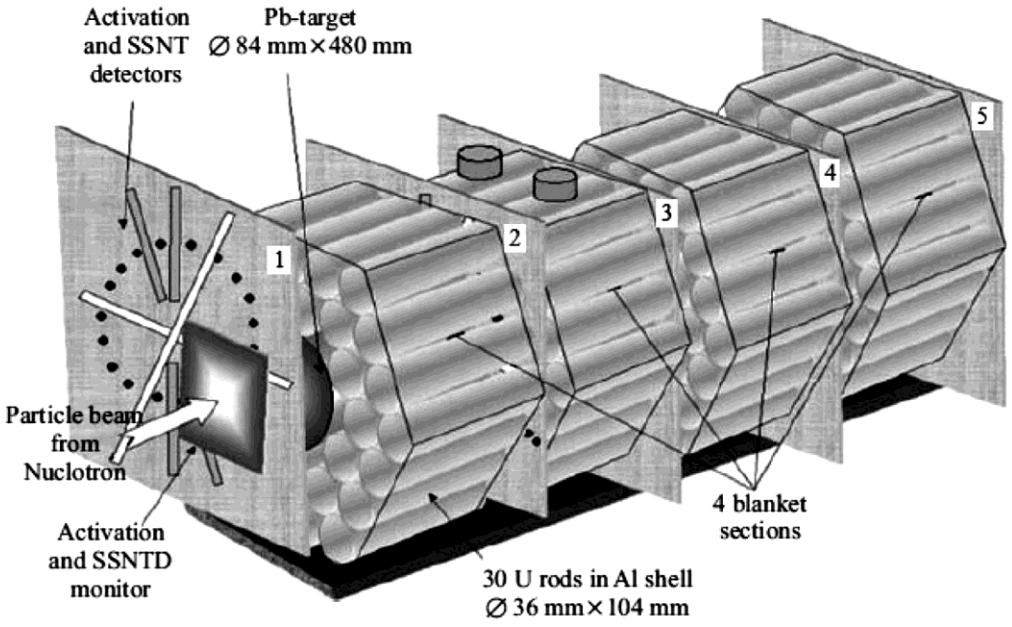

Fig. 1 — Schematic drawing of the E+T target. Numbers 0-4 represent locations for activation detectors placement, i.e., no. 1 is the location in front of the target, no. 2-4 are gaps between the sections and no. 5 is the location behind the target.

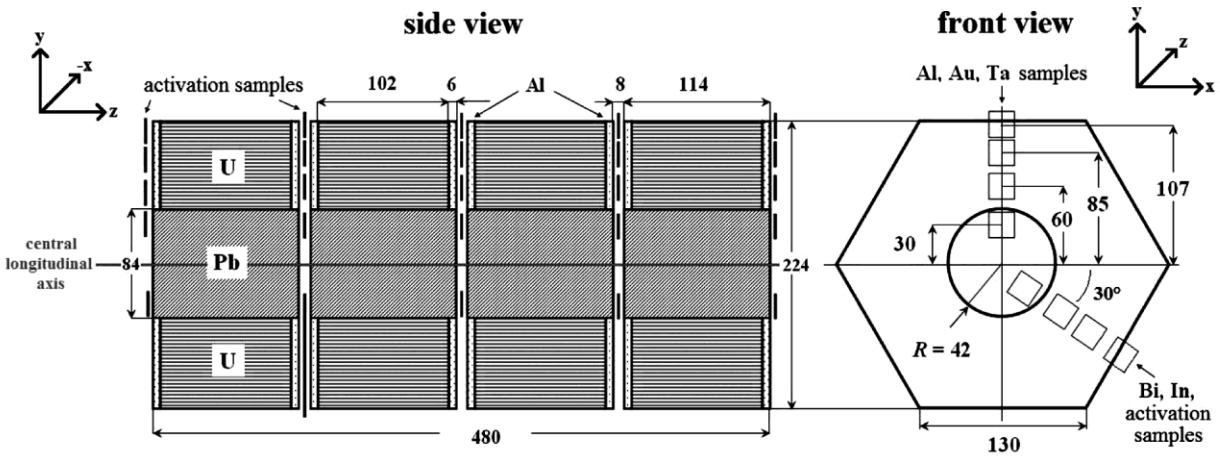

Fig. 2 — Positions of activation samples in the E+T assembly during 1.6 GeV deuteron irradiation. Dimensions are in mm.

The assembly was irradiated with the 1.6 GeV deuteron beam of the Nuclotron accelerator at JINR for 6.7 hours. The integral number of deuterons impinging on the target was determined by aluminum activation monitors using ^{27}Al(d, 3p+2n)^{24}Na reaction[8] and concentric aluminum rings[9]. The coordinates on the setup entrance of the source beam center and spatial beam profile of the impinging beam were determined by Solid-State Nuclear Track Detectors[10] (SSNTD) and a set of copper activation foils[11]. For more detail information, see[12]. The integral number of deuterons impinging on the target were measured as 2.45×10^{13}. The coordinates of the beam center (d_x, d_y) on the target entrance and full widths at half maximum of the 2D Gaussian profile are given in Table 1. These beam characteristics are also used as input parameters for the simulations.

The placement of activation samples in the E+T experiment is given in Fig. 2. The samples are mounted on plastic holders inserted in front of, behind, and between the E+T sections at longitudinal distances of 0, 11.8, 24.0, 36.2, and 48.4 cm from the target front. On the holders, the samples are placed in radial distances of 3.0, 6.0, 8.5, and 10.7 (upward direction) or 11.5 cm (right-down direction) from the central longitudinal axis. The first group of samples (^{27}Al, ^{197}Au, ^{181}Ta grouped together) is positioned in the upward direction, and the second group of samples (^{209}Bi + ^{115}In) is positioned in the right-down direction. The samples are of a square shape with a side length of 20 mm for ^{27}Al, ^{197}Au and ^{181}Ta samples, 25 mm for ^{209}Bi samples, and 12.5 mm for ^{115}In samples. The average weights of the samples are 0.6 g for ^{27}Al, 0.3 g for ^{197}Au, 0.8 g for ^{181}Ta, 6.5 g for ^{209}Bi and 0.6 g for ^{115}In.

Table 1 — Beam characteristics of the E+T, QUINTA, and BURAN experiments/simulations. d_x and d_y are coordinates of the beam center position, and $FWHM_x$ and $FWHM_y$ are full energy widths at half maximum of the 2D beam Gaussian profile.

Experiment	d_x(cm)	d_y(cm)	$FWHM_x$(cm)	$FWHM_y$(cm)
E+T	-0.64	-0.39	2.87	1.92
QUINTA	1.31	0.76	3.40	3.97
BURAN	0.00	0.00	3.50	3.50

About this experiment was already written in earlier study[12]. In this paper, we present only some preliminary results of a newly prepared systematics about E+T experiments[13],which will be published later in a separate paper.

2.2 QUINTA assembly

The QUINTA assembly (see Figs 3 and 4) consists of natural uranium rods, which are arranged into five hexagonal sections with an inscribed circle diameter of 284 mm. The diameter of a single rod is 36 mm, the length is 104 mm, and the weight is 1.72 kg. In the first section, there is an air channel with a diameter of 80 mm, serving as a beam window. The activation samples are fixed to aluminum holders, which are positioned in front of and behind the uranium sections and in 17 mm air gaps between the sections. A 100 mm-thick lead shielding covers the QUINTA assembly. On the front side of the shielding, there is a beam entrance. A more detailed description of the QUINTA assembly is given, e.g. in earlier study[7].

In this paper, an irradiation of the QUINTA assembly with the 660 MeV proton beam of the Phasotron accelerator is presented. The beam intensity delivered by the Phasotron is approximately 10^{13} protons.s^{-1}, which is two orders of magnitude higher

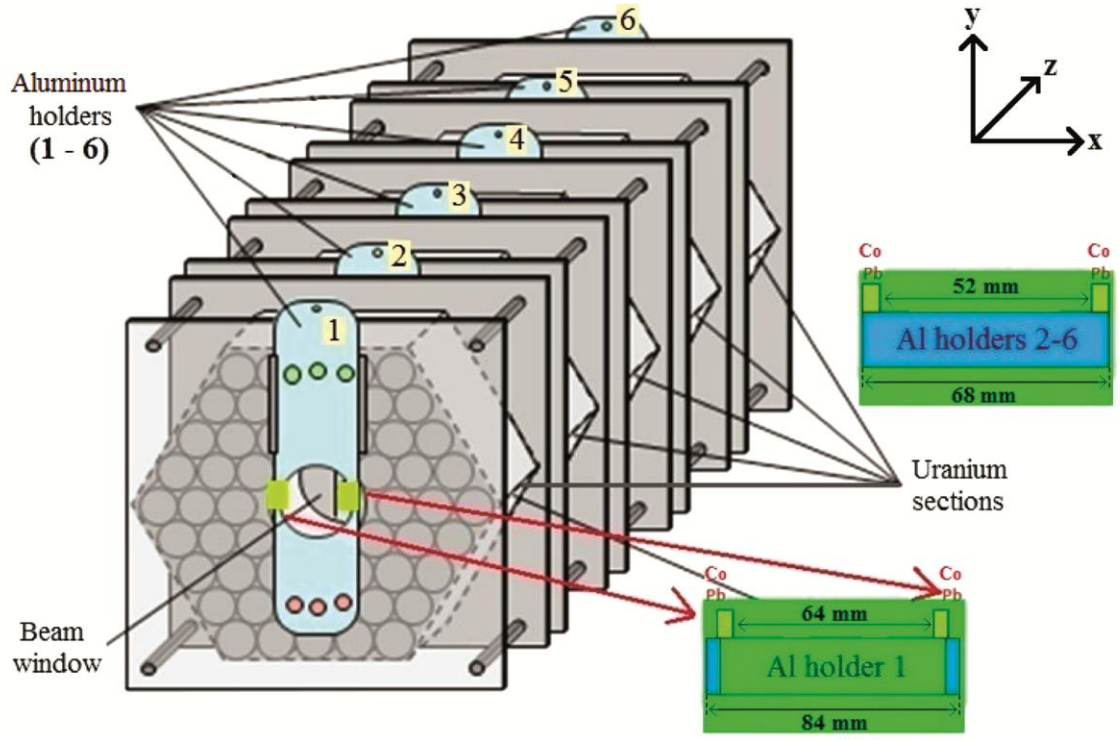

Fig. 3 — Schematic drawing of the QUINTA assembly and placement of the ^{59}Co and ^{nat}Pb activation samples on aluminum holders.

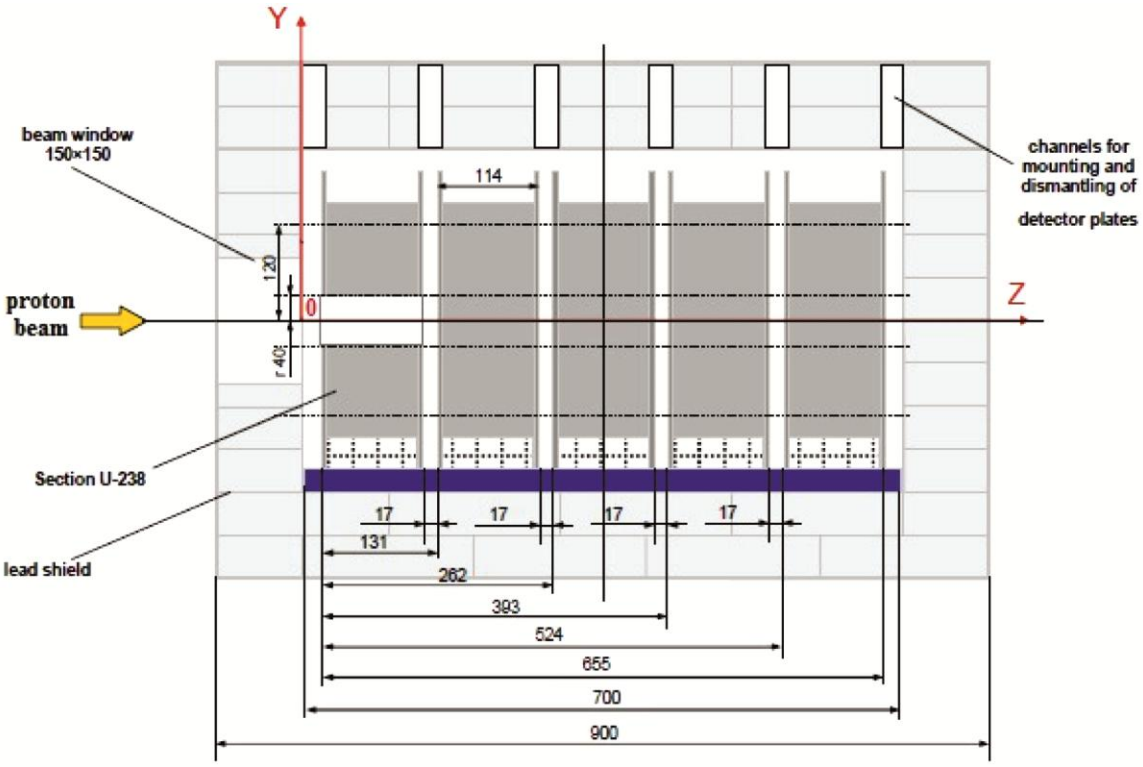

Fig. 4 — Cross-cut of the QUINTA assembly surrounded by the lead shielding. Dimensions are in mm

than from the Nuclotron. The beam characteristics of the QUINTA experiment are given in Table 1. The coordinates of the source beam center and spatial beam profile on the assembly entrance were measured by an ionization chamber[15]. The integral number of protons impinging on the target was 3.38×10^{15}. It was determined using the aluminum activation monitors and $^{27}Al(p, 3p+n)^{24}Na$ reaction. The irradiation time was 4.6 hours. The activation samples of ^{59}Co and ^{nat}Pb (grouped together) were located on the left and right side of the aluminum holders (see Fig. 3). The dimensions of the ^{59}Co and ^{nat}Pb samples were 8×25 and 8×20 mm, respectively. The masses of ^{59}Co and ^{nat}Pb samples were 1.90 and 0.51 g on average, respectively.

Activation samples of ^{59}Co and ^{nat}Pb were chosen as a convenient combination for investigation of the mixed neutron-proton field along the beam passage. We evaluated the production of ^{58}Co isotope (emerged by neutron- and proton-induced reactions with the ^{59}Co material) and production of the ^{206}Bi isotope (emerged only by proton-induced reactions with the ^{nat}Pb material). Because the ^{206}Bi production is not influenced by the neutron-induced reactions, ^{nat}Pb samples are suitable for monitoring the primary proton beam.

The number of reactions in the left and right positioned samples is supposed to differ due to 2-degree QUINTA rotation along the QUINTA geometry center (see Fig. 5) and the accelerator settings. The meaning of the rotation is in maximal use of the proton beam, i.e., the protons fully hit the uranium rods and do not pass through the air space between the rods behind the target without interaction.

2.3 BURAN assembly

As a successor of QUINTA is considered to be the BURAN assembly (see Fig. 6). BURAN is supposed to be a "quasi-infinite" spallation target, which means that there should be a minimum neutron leakage from

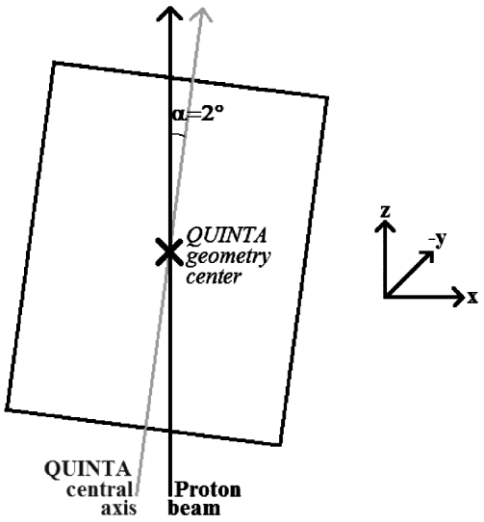

Fig. 5 — QUINTA rotation along its geometry center.

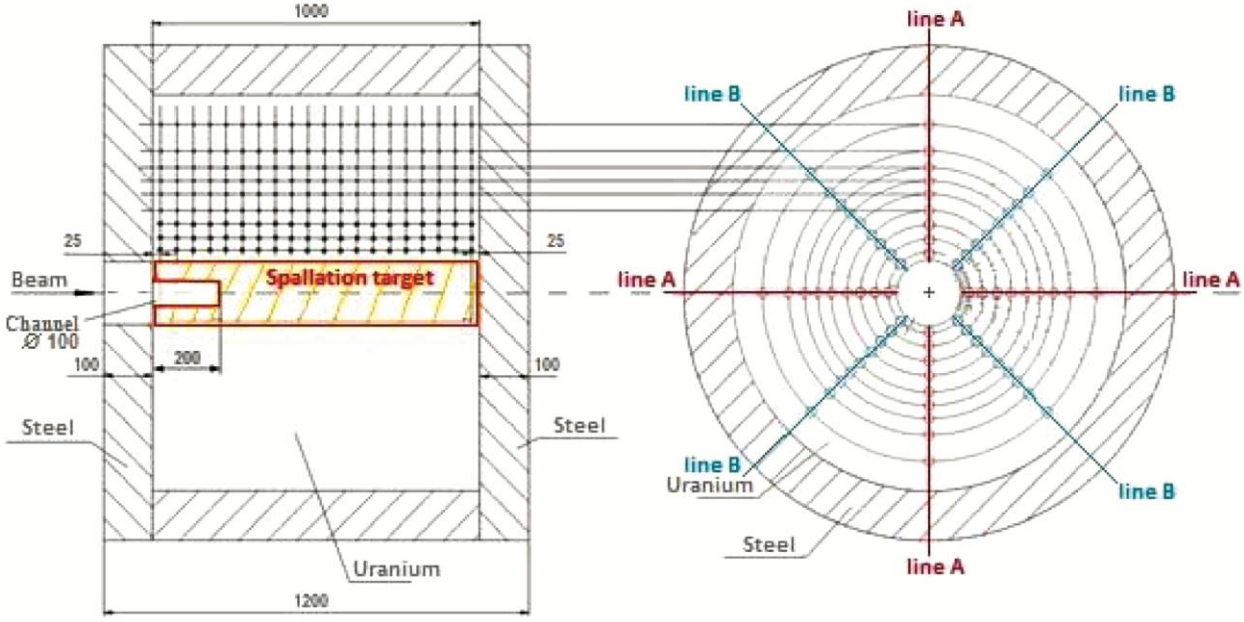

Fig. 6 — Schematic drawing of the BURAN assembly. Dimensions are in mm.

the assembly. According to our simulations with MCNPX 2.7.0, the neutron leakage in the case of BURAN irradiated with the 660 MeV protons is 15 %, while the leakage in the case of QUINTA is 76 %. Experiments of BURAN irradiation with the 660 MeV proton beam of the Phasotron are now in the preparatory phase at JINR.

The BURAN assembly consists of a large depleted uranium (containing 0.3 % of ^{235}U) blanket of 1200 mm in diameter and 1000 mm in length with a total uranium mass of 20 tons. The cylinder has a 200 mm in diameter air opening in its center, in which a spallation target can be inserted. The target can be of different spallation materials like lead, carbon or uranium. The blanket is shielded with a 100 mm steel layer, having a 200 mm in diameter beam window.

The blanket is equipped with 72 air channels of 30 mm in diameter parallel to the beam axis, and 20 measuring positions are defined in every channel. Totally 1440 positions are supposed to enable outstanding flexibility in neutron spatial and spectral distribution measurement. The radial distances of the air channels from the BURAN central longitudinal axis are: 140, 180, 220, 260, 300, 340, 380, 440 and 520 mm (lines A), and 120, 160, 200, 240, 280, 320, 360, 400 and 480 mm (lines B).

2.4 Data analysis

The gamma-ray spectra of the irradiated activation samples were measured with HPGe detectors and analyzed by the DEIMOS32 computation tool[16]. The radionuclide production in the samples was evaluated by gamma-spectrometry techniques. The radionuclide production is characterized by the quantity called reaction rate R, which represents the number of nuclei emerging per a primary particle and an atom of the sample material.

R is given by Eq. (1), involving all necessary spectrometry corrections[17].

$$R = \frac{S(E_\gamma)}{m_s}\cdot\frac{M}{N_A}\cdot\frac{1}{I_p}\cdot\frac{1}{I_\gamma}\cdot\frac{t_{real}}{t_{live}}\cdot\frac{C_B\cdot C_{abs}}{\varepsilon_p(E_\gamma)\cdot C_g\cdot COI}\cdot\frac{\exp(\lambda\cdot t_{delay})}{1-\exp(-\lambda\cdot t_{real})}\cdot\frac{\lambda\cdot t_{irr}}{1-\exp(-\lambda\cdot t_{irr})} \quad \ldots (1)$$

$S(E_\gamma)$ is the area of gamma peak, m_s is the mass of activation sample, M is the relative atomic mass of the activation material, N_A is the Avogadro number, I_p is the integral number of primary particles impinging on the target, I_γ is the intensity of gamma transition, t_{irr} is the time of irradiation, t_{delay} is the time between end of the irradiation and beginning of the measurement, t_{real} is the real measurement time, t_{live} is the live measurement time, λ is the decay constant, $\varepsilon_p(E_\gamma)$ is the peak efficiency of the HPGe detector, C_B is the beam instability correction factor, C_{abs} is the correction for self-absorption of gamma photons, C_g is the correction on activation sample geometry and COI is the correction factor on real γ–γ cascade coincidences. More details about the data evaluation and the measurement procedure can be found in[14].

2.5 Simulation procedure

The simulations were performed using the Monte Carlo-based code MCNPX 2.7.0[18]. We developed complex geometry models of the E+T, QUINTA, and BURAN assemblies, including the shielding. Small volumes, representing the activation samples were defined to the positions in which the samples were situated in the real experiments. The flux of neutrons and protons (and also deuterons in case of the E+T experiment) was tallied in the small volumes. The tabular cross-sections of the standard library ENDF/B-VII.1[19] were engaged in combination with the physics models INCL4.2[20] (Intranuclear Cascade model) and ABLA-KHSv3p[21] (Fission-Evaporation model).

The cross-sections of the particular threshold reactions in the E+T samples were extracted from the deterministic code TALYS 1.8[22] employing the Constant Temperature model coupled with the Fermi Gas model, and above 200 MeV from MCNPX 2.7.0 using the INCL4.2 and CEMO3[26] models. The cross-sections of the threshold reactions for the QUINTA and BURAN simulations were extracted from TALYS 1.6[23], employing the Constant Temperature+Fermi Gas model combination.

The simulated reaction rates R_{sim} of the particular activation products were acquired by folding of the simulated flux and the calculated cross-sections according to the following equation:

$$R_{sim} = \sum_{i=n,p,d}\sum_{E_{thr}}^{E_{beam}}\sigma_i(\Delta E)\cdot\varphi_i(\Delta E) \quad \ldots (2)$$

where $\sigma_i(\Delta E)$ and $\varphi_i(\Delta E)$ are the reaction cross-section and the flux, respectively, for neutrons n, protons p and deuterons d (deuteron contributions are involved only in the E+T simulations) in the energy interval ΔE. The intervals ΔE range from the effective threshold energy E_{thr} up to the energy of the primary beam E_{beam}, i.e. E_{beam}=1.6 GeV in the E+T simulations

and E_{beam}=660 MeV in the QUINTA and BURAN simulations.

The statistical uncertainties of the simulation results were usually below 5 %, and therefore, they could be neglected. The statistical and systematical uncertainties of the experimental results were taken into consideration, and they are visible in the graphs.

3 Results and Discussion

Experiment-to-simulation ratios of the radial reaction rates in ^{209}Bi activation samples at a longitudinal distance of 11.8 cm in the E+T assembly are given in Fig. 7. There is a fairly good agreement between the experiment and MCNPX simulation. The shape of the radial distributions of different isotopes production is described by MCNPX quite well, although MCNPX overestimates the experiment in most cases. The experimental/simulation agreement generally looks worse for low radial positions, i.e., positions close to the central beam axis. Proton- or deuteron-induced reactions, and asymmetry given by the beam position and shape are mostly present in the beam passage region and close to it. The importance of these reactions and asymmetry fades away with growing radial distance in favor of neutron-induced reactions. It means that samples close to the primary beam passage are sensitive to the precision of the accelerator beam settings more than samples located outside this region. The biggest disagreement of experimental and simulated data in the region close to the beam passage indicates that a very important factor for the experiments and the consequent simulation benchmarks is the precision of the accelerator beam settings and the primary beam geometry description. For this reason, we focused on the investigation of the region close to the beam passage and the study of the beam settings influence on the QUINTA assembly experiments.

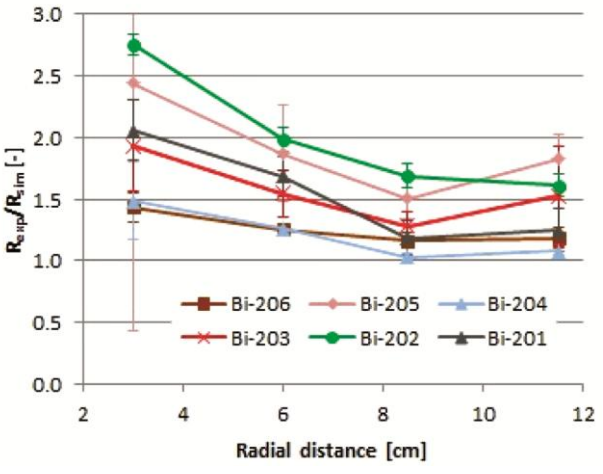

Fig. 7 — Experimental and simulated reaction rate ratios R_{exp}/R_{sim} for isotopes of Bi produced in ^{209}Bi samples at a longitudinal distance 11.8 cm in E+T. Lines between the points have no physical meaning, and they are present just to guide a reader's eye.

The reaction rates of ^{58}Co and ^{206}Bi production in activation samples of ^{59}Co and ^{nat}Pb on the left and right sides in QUINTA and simulated results of proton contributions to the ^{58}Co reaction rates are presented in Fig. 8. Some results of this experiment were already published[24].

The proton contribution for the first point of ^{58}Co on the right side in Fig. 8. reaches almost 70 %. This indicates that, according to simulations, the corresponding ^{59}Co sample was hit by the primary beam in a great measure. However, this is not confirmed by the experimental data of ^{206}Bi from Fig. 8.b. The production of ^{206}Bi in the first position on the right side should, therefore, be much greater than on the left side, which was not observed. This discrepancy corresponds to the experiment/simulation ratio in Fig 8.d for the ^{206}Bi on the left side, where the simulation is greatly underestimated. ^{206}Bi is only produced in proton-induced reactions and therefore is more sensitive to the proton beam settings. This indicates that there is uncertainty in the beam geometry description.

The agreement between experimental and simulated reaction rates of the ^{58}Co and ^{206}Bi production in Fig. 8.d is relatively good, except for the first and last points for the left side. The edge values are very sensitive not only to inaccuracies of the accelerator settings, but also to systematical and statistical errors.

The results for activation samples close to the central beam axis are very sensitive to the beam accelerator settings, especially to the beam center coordinates and angle of the QUINTA rotation. Therefore, an investigation of the parameter changes was performed for the QUINTA experiment. The coordinate d_x was being systematically changed from 0.4 up to 3.0 cm (Figs. 9 and 10), and the beam was being rotated from angle α=0° up to 4° (Figs. 11 and 12). Simulated reaction rates of ^{58}Co and ^{206}Bi on the left and right sides were studied. Note that the angle of beam rotation α=2° corresponds to the QUINTA 2-degree rotation, and from this position, the beam was being deflected up to ±2° in the plane xz.

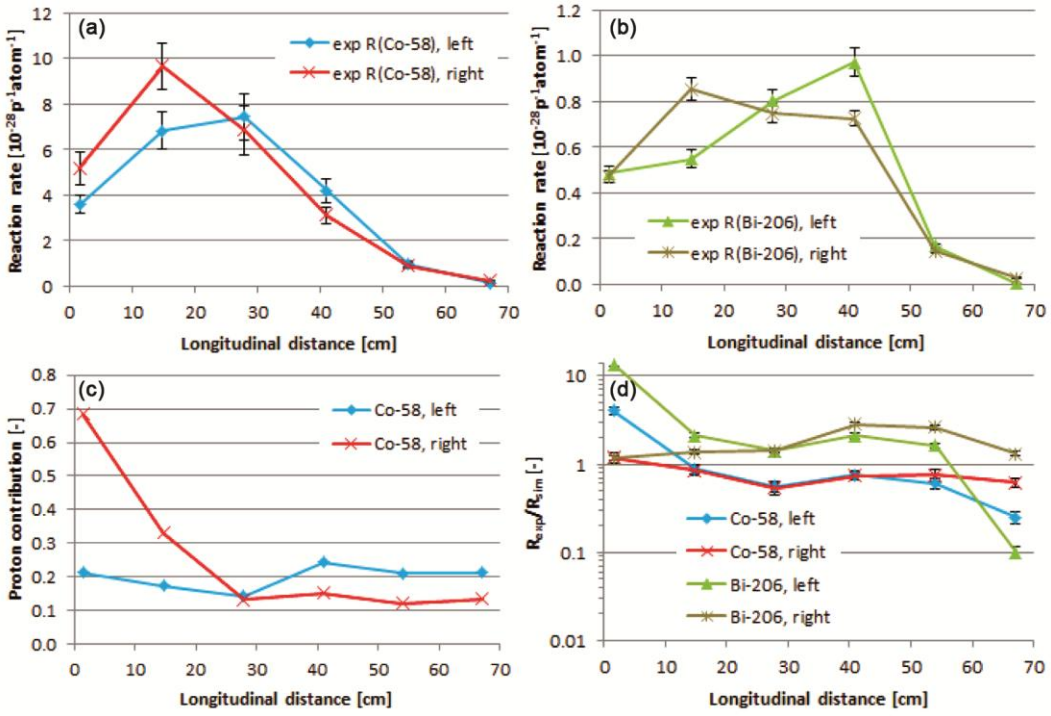

Fig. 8 — Experimental reaction rates of ^{58}Co production (a) and ^{206}Bi production (b) for activation samples on the left and right sides in QUINTA, simulated results of proton contributions to the ^{58}Co reaction rates (c), and experimental and simulated reaction rate ratios R_{exp}/R_{sim} of the ^{58}Co and ^{206}Bi products (d).

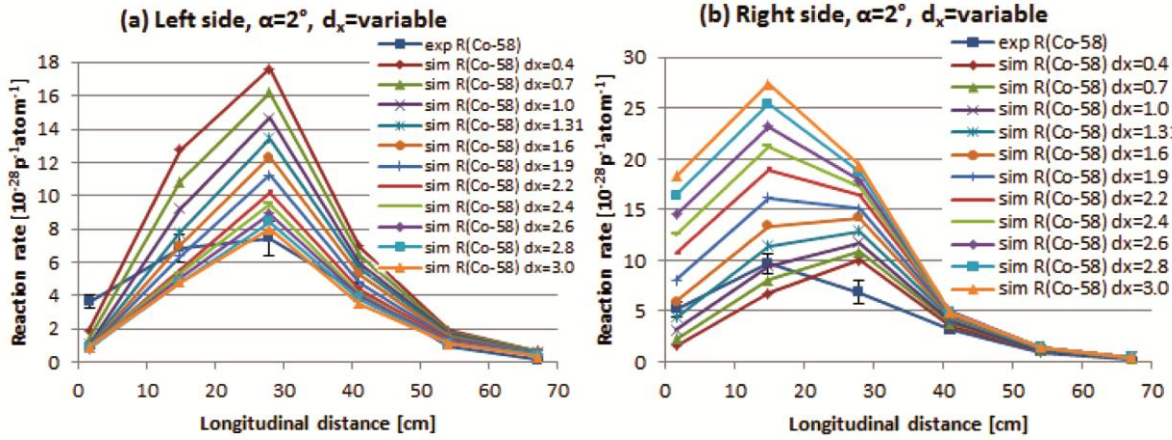

Fig. 9 — Simulated reaction rates with variable coordinate d_x and angle α=2° of ^{58}Co production for samples on the left (a) and right (b) side in QUINTA.

From Figs 9 and 10, where the beam angle α was at a constant value of 2° and the beam coordinate d_x was being shifted, one can notice that reaction rate maxima on the left side graphs are being shifted forward (in the direction of greater longitudinal distance) with raising coordinate d_x of the beam center. On the right side graphs, the situation is the opposite. It is a consequence of the 2-degree QUINTA rotation.

We also investigated the effect of beam parameters changes on activation samples not close to the beam passage. For this purpose, we redefined the studied samples in the MCNPX model to more remote positions and performed simulations. The imaginary ^{59}Co and ^{nat}Pb samples were placed 12 cm in the vertical direction above their original positions. The results for the ^{58}Co production are given in Figs 13 and 14. The effect of beam parameters changes is

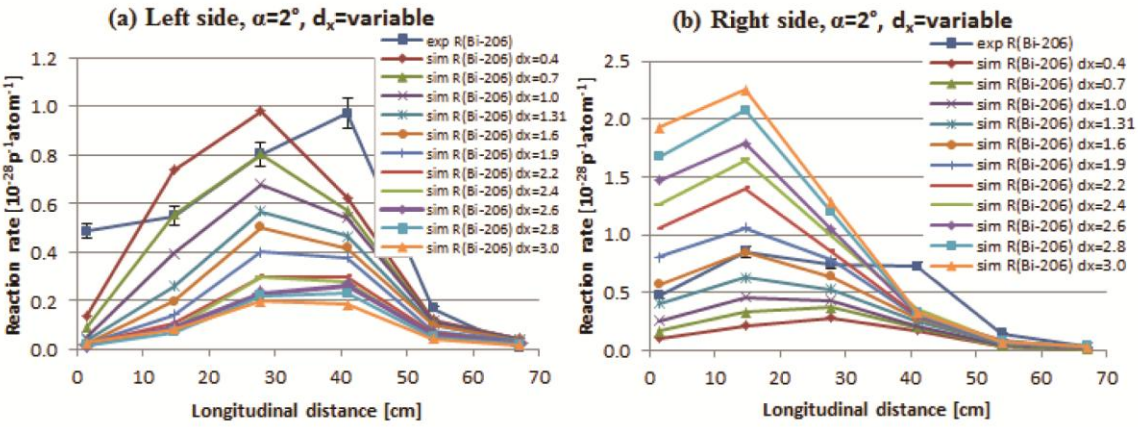

Fig. 10 — Simulated reaction rates with variable coordinate d_x and angle α=2° of ^{206}Bi production for samples on the left (a) and right (b) side in QUINTA.

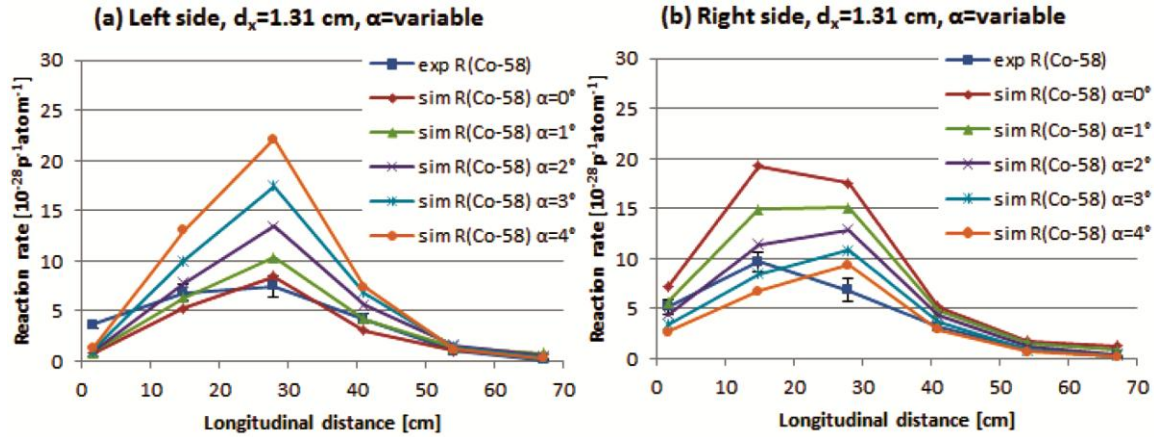

Fig. 11 — Simulated reaction rates with coordinate d_x=1.31 cm and variable angle α of ^{58}Co production for samples on the left (a) and right (b) side in QUINTA.

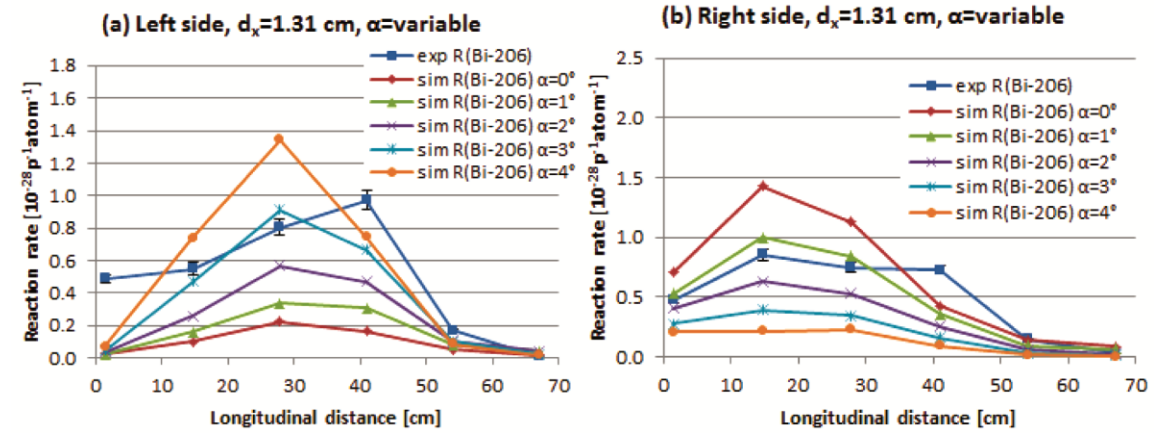

Fig. 12 — Simulated reaction rates with coordinate d_x=1.31 cm and variable angle α of ^{206}Bi production for samples on the left (a) and right (b) side in QUINTA.

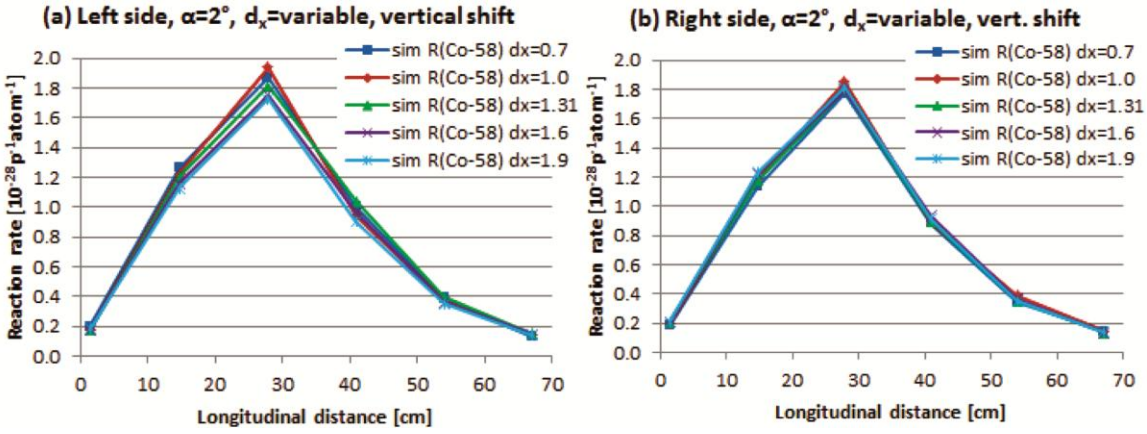

Fig. 13 — Simulated reaction rates with variable coordinate d_x and angle α=2° of ^{58}Co production for imaginary samples (vertically shifted 12 cm above their original positions) on the left (a) and right (b) side in QUINTA.

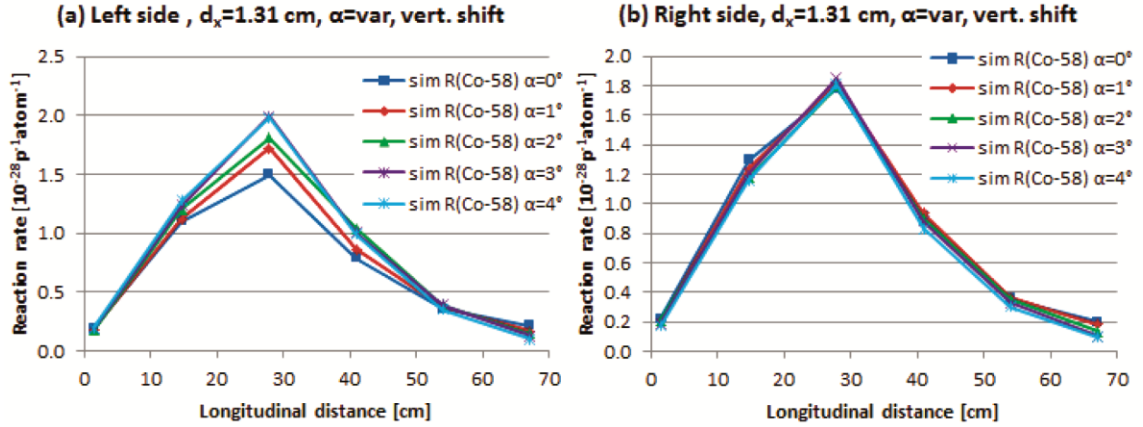

Fig. 14 — Simulated reaction rates with coordinate d_x=1.31 cm and variable angle α of ^{58}Co production for imaginary samples (vertically shifted 12 cm above their original positions) onthe left (a) and right (b) side in QUINTA.

much smaller than in Figs 9 and 11, where the samples were situated close to the central beam passage. The average change in reaction rate derived from the values in Fig. 13 is around 1.4 % per 1 mm beam shift. The influence of protons can be considered negligible in the positions remote from the primary beam axis, because of the absence of the primary protons. Also, the intensity of the neutron field in these positions is not very sensitive to the neutron source location changes. The usage of MCNPX 2.7.0 for simulations of QUINTA positions not close to the central beam axis was also demonstrated in our previous paper[25] for ^{59}Co, ^{197}Au, and ^{209}Bi activation detectors.

Based on the knowledge that the influence of inaccuracies of beam parameters settings do not affect in great measure the neutron production in the QUINTA remote radial positions, we assume that the future BURAN experiments will be suitable for benchmarks considering the fact that in the experiments activation samples will be situated not close to the primary beam passage. To verify this hypothesis, we performed simulations on BURAN irradiated by the 660 MeV proton beam. Cylindrical volumes of 30 mm in diameter and 10 mm in length, representing ^{59}Co activation samples, were added to the BURAN geometry model into the first air channel in the upward direction to every measurement position, i.e., 20 ^{59}Co volumes were situated 14 cm above the central longitudinal axis in line A. Simulations were performed for BURAN equipped with a lead spallation target. A beam channel of 100 mm in diameter and 200 mm in length was defined in the lead target front (see Fig. 6). The coordinates of the beam center (d_x, d_y) on the BURAN entrance and full widths at half maximum of the 2D

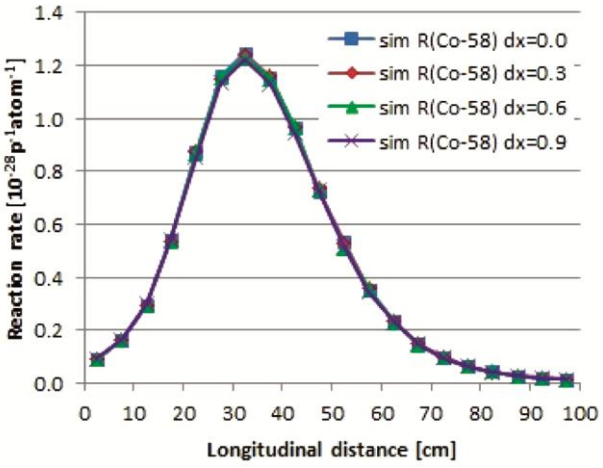

Fig. 15 — Simulated reaction rates with variable coordinate d_x of ^{58}Co production for imaginary samples in BURAN.

Gaussian profile used as input parameters for the simulations are given in Table 1. Coordinate d_x was being changed from 0 to 0.9 cm. The simulation results for the ^{58}Co production given in Fig. 15 show very little differences in reaction rates for the considered beam displacements. The average change in reaction rate derived from the given values is around 0.6 % per 1 mm beam shift.

4 Conclusions

Using activation samples positioned near the primary beam, we measured neutron and proton production in uranium spallation experiments at assemblies E+T irradiated by the 1.6 GeV deuteron beam and QUINTA irradiated by the 660 MeV proton beam. The experiments were compared to the Monte Carlo simulations performed with MCNPX 2.7.0, which was also used to study the sensitivity of the results to the accuracy of primary beam parameters.

On the QUINTA irradiation results, we demonstrated that the intensity of the mixed neutron-proton field close to the primary beam passage is very sensitive to accelerator beam settings. Monte Carlo simulation benchmarks in this region are, therefore, possible only under the condition of a very accurate primary beam geometry description. The beam proximity influence is greater for the ^{206}Bi isotope produced in ^{nat}Pb samples than for the ^{58}Co isotope produced in ^{59}Co samples, due to the fact that ^{206}Bi is mostly produced by the primary beam protons. We confirmed that there exist inaccuracies in the primary beam geometry description, and we plan to develop universal correction factors for the beam settings that could be applied to the experiments in order to make the settings more precise.

It was also proven that the influence of inaccuracies of beam parameter settings for neutron production is less significant for remote radial positions in the QUINTA assembly. We also proved that the significance of a possible beam displacement in the future BURAN experiments on the reaction rate activation measurements would be negligible. Therefore, the experiments will be very useful for benchmark studies of Monte Carlo simulation codes.

References

1 Vasilkov R G, Goldanskii V I, Grishkevich Y V, Lupandin, O S & Pimenov B A, *Atom Energy*, 25 (1968) 1307.

2 Malakhov A I, *Nucl Phys A*, 734 (2004) 82.

3 Dzhelepov V P, Dmitrievsky V P & Onishchenko L M, *IEEE Trans Nucl Sci*, 30 (1983) 2134.

4 Adam J, Balabekyan A, Bradnova V, Brandt R, Golovatiouk V M, Katovský K, Krivopustov M I, Kalinnikov V G, Odoj R, Pronskikh V S, Robotham H, Siemon K, Solnyshkin A A, Stegailov V I, Tsoupko-Sitnikov V M, Vladimirova N M & Westmeier W, *Nucl Instr Meth A*, 562 (2006) 741.

5 Adam J, Bhatia C, Katovský K, Kumar V, Majerle M, Pronskikh V S, Khilmanovich A M, Martsynkevich B A, Zhuk I V, Golovatiouk V M, Westmeier W, Solnyshkin A A, Tsoupko-Sitnikov V M & Potapenko A S, *Eur Phys J A*, 47 (2011) 85.

6 Krivopustov M I, Chultem D, Adam J, Kalinnikov V G, Pavliouk A V, Perelygin V P, Polanski A, Sosnin A N, Sereter Z, Zaverioukha O S, Tumendelger T, Gerbish S, Ganzorig Z, Kaznovski P S, Kasnovski S P, Lobanov S G, Mischenkov V F, Fonarev B I, Shapovalov Y L, Odoj R, Chigrinov S E, Khilmanovich A M, Kievets M K, Korneev S V, Lomonosova E M, Martsinkevich B A, Zhuk I V, Langrock E J, Voronkov A V, Brandt R, Robotham H, Vater P, Westmeier W, Bielewicz M, Szuta M, Strugalski Z, Wojciechowski A, Kugler A, Wagner V, Hashemi-Nezhad S R, Zamani-Valasiadou M, Adloff J, Debeauvais M & Dwivedi K K, *Kerntechnik*, 68 (2003) 48.

7 Furman W I, Adam J, Baldin A A, Berlev A I, Gundorin N A, Khushvaktov J H, Kadykov M G, Kopatch Y N, Kostyukhov E V, Kudashkin I V, Makan'kin A M, Mar'in I I, Polansky A A, Pronskikh V S, Rogov A D, Schegolev V Y, Solnyshkin A A, Tsoupko-Sitnikov V M, Tyutyunnikov S I, Vishnevsky A V, Vladimirova N M, Wojciechowski A, Závorka L, Chilap V V, Chinenov A V, Dubinkin B, Fonarev B I, Galanin M V, Kolesnikov V, Solodchenkova S A, Artyushenko M Y, Sotnikov G V, Voronko V A, Khilmanovich A M, Martsynkevich B A, Kislitsin S B, Kvochkina T N, Zhdanov S V, Husak K V, Korneev S V, Potapenko A S, Safronova A A, Zhuk I V, Suchopár M, Svoboda O, Vrzalová J, Wagner V, Kostov L, Stoyanov C, Zhivkov P, Bielewicz M, Kilim S, Strugalska-Gola E, Szuta M, Westmeier W, Manolopoulou M &

Hashemi-Nezhad S R, *Proc XXI Int Baldin Sem High Energy Phys Probl*, Dubna, Russia, PoS, 173 (2012) 086.

8 Suchopár M, Wagner V, Svoboda O, Vrzalová J, Chudoba P, Kugler A, Adam J, Závorka L, Baldin A A, Furman W I, Kadykov M G, Khushvaktov J H, Solnyshkin A A, Tsoupko-Sitnikov V M & Tyutyunnikov S I, *Nucl Instr Meth B*, 344 (2015) 63.

9 Westmeier W, Experiment S: 4.00 GeV Deuterons on E+T, Technical Report, Du-Ma Collaboration, 2011.

10 Zhuk I V, Bukhal O V, Husak K V, Safronova A A, Patapenka A A, Artyushenko M Y, Sotnikov G V, Voronko V A, Tyutyunnikov S I, Furman W I, Kadykov M G, Chinenov A V & Chilap V V, *Proc 12th Int Sch Sem Act Probl Microw Phys*, Gomel, Belarus, 1 (2015) 181.

11 Svoboda O, *Experimental study of neutron production and transport for ADTT*, PhD thesis, Czech Technical University in Prague, 2011.

12 Svoboda O, Adam J, Bielewicz M, Kilim S, Krása A, Krivopustov M I, Majerle M, Stegailov V I, Strugalska-Gola E, Solnyshkin A A, Szuta M, Tsoupko-Sitnikov V M & Wagner V, *JINR Preprint*, E15-2011-39, 2011.

13 Krása A, Wagner V, Majerle M, Křížek F, Kugler A, Svoboda O, Adam J & Krivopustov M I, *Nucl Instr Meth A*, 615 (2010) 70.

14 Suchopár M, Wagner V, Svoboda O, Vrzalová J, Chudoba P, Tichý P, Majerle M, Krása A, Kugler A, Adam J, Závorka L, Baldin A A, Furman W I, Kadykov M G, Khushvaktov J H, Solnyshkin A A, Tsoupko-Sitnikov V M & Tyutyunnikov S I, *Nucl Instr Meth A*, 908 (2018) 347.

15 Adam J, Baldin A A, Vladimirova N M, Gundorin N A, Gus'kov B N, Dyachenko V M, Elishev A F, Kadykov M G, Kostyuhov E, Krasnov V A, Mar'in I I, Pronskikh V S, Rogov A D, Solnyshkin A A, Stegailov V I, Stetsenko S G, Tyutyunnikov S I, Furman W I, Tsoupko-Sitnikov V M, Belov E M, Galanin M V, Kolesnikov V A, Ryazansky N-M, Solodchenkova S A, Fonarev B I, Chilap V V, Chinenov A V, Baldina E, Balabekyan A, Karapetyan G, Zhuk I V, Korneev S V, Potapenko A S, Safronova A A, Sorokin V N, Sorokin V V, Khilmanovich A M, Marcynkevich B A, Korbut T N, Stoyanov C, Kostov L, Zhivkov P, Yordanov O, Batzev S, Protohristov C, Kugler A, Wagner V, Majerle M, Krása, Svoboda O, Katovský K, Šťastný O, Tuleushev A, Gudima K, Baznat M, Togoo R, Otgonsuren D, Tumendelger T, Damdinsuren T, Szuta M, Strugalska-Gola E, Kilim S, Bielewicz M, Wojciechowski A, Voronko V A, Sotnikov G V, Sidorenko D Y, Haysak I, Hashemi-Nezhad S R, Borger Y, Westmeier W, Robotham H, Ensinger W, Severin D, Rossbah M, Thomauske B, Zamani-Valasiadou M, Manolopoulou M, Stoulos S, Fragopolou M, Jokic S, Kumawat H, Kumar V & Sharma M, *JINR Preprint*, E10-2010-61, 2010.

16 Frána J, *J Radioanal Nucl Chem*, 257 (2003) 583.

17 Majerle M, Krása A, Svoboda O, Adam J, Peetermans S, Sláma O, Stegailov V I, Tsoupko-Sitnikov V M & Wagner V, *JINR Preprint*, E11-2009-178, 2009.

18 Pelowitz D B, MCNPX version 2.7.0, User Manual, LA-CP-11-00438, 2011.

19 Chadwick M B, Herman M, Obložinský P, Dunn M E, Danon Y, Kahler A C, Smith D L, Pritychenko B, Arbanas G, Arcilla R, Brewer R, Brown D A, Capote R, Carlson A D, Cho Y S, Derrien H, Guber K, Hale G M, Hoblit S, Holloway S, Johnson T D, Kawano T, Kiedrowski B C, Kim H, Kunieda S, Larson N M, Leal L, Lestone J P, Little R C, McCutchan E A, MacFarlane R E, MacInnes M, Mattoon C M, McKnight R D, Mughabghab S F, Nobre G P A, Palmiotti G, Palumbo A, Pigni M T, Pronyaev V G, Sayer R O, Sonzogni A A, Summers N C, Talou P, Thompson I J, Trkov A, Vogt R L, Marck S C, Wallner A, White M C, Wiarda D & Young P G, *Nucl Data Sheets*, 112 (2011) 2887.

20 Boudard A, Cugnon J, Leray S & Volant C, *Phys Rev C*, 66 (2002) 044615.

21 Junghans A R, Jong M, Clerc H G, Ignatyuk A V, Kudyaev G A & Schmidt K H, *Nucl Phys A*, 629 (1998) 635.

22 Koning A, Hilaire S & Goriely S, TALYS-1.8, User Manual, 2015.

23 Koning A, Hilaire S & Goriely S, TALYS-1.6, User Manual, 2003.

24 Tichý P, Adam J, Baldin A A, Chudoba P, Furman W I, Gustov S A, Khushvaktov J H, Mar'in I I, Solnyshkin A A, Suchopár M, Svoboda J, Tyutyunnikov S I, Vespalec R, Vrzalová J, Wagner V, Závorka L & Zeman M, *Proc 26th Int Nucl Phys Conf*, Adelaide, Australia, PoS, 281 (2017) 115.

25 Závorka L, Vrzalová J, Zeman M, Adam J, Čaloun P, Chudoba P, Furman W I, Katovský K, Khushvaktov J H, Solnyshkin A A, Suchopár M, Tichý P, Tsoupko-Sitnikov V M, Tyutyunnikov S I, Vespalec R & Wagner V, *Nucl Instr Meth A*, 903 (2018) 246.

26 Mashnik S G, Gudima K K, Prael R E, Sierk A J, Baznat M I & Mokhov N V, *LANL report*, LA-UR-082931, 2008.